S.1 Sea Salt Source functions

In order to combine, compare and integrate the functions introduced below some general assumptions and transformations are necessary that are described in Eqs. (1), (2), and (3). According to Lewis and Schwartz (2004) we assume

$$r_{80} = 2 \times r_{\text{dry}} = D_{\text{dry}} \tag{1}$$

Following the above relation and basic calculus we get

$$\frac{dF}{dr_{80}} = \frac{dF}{dD_{\text{dry}}} \tag{2}$$

$$\frac{dF}{dD_{\text{dry}}} = \frac{d\ln D_{\text{dry}}}{dD_{\text{dry}}} \times \frac{dF}{d\ln D_{\text{dry}}} = \frac{1}{D_{\text{dry}}} \times \frac{dF}{d\ln D_{\text{dry}}} = \frac{1}{\ln 10 \times D_{\text{dry}}} \times \frac{dF}{d\log_{10} D_{\text{dry}}} \tag{3}$$

S.2 MO86, SM93, GO03, MA03, and SP13

Monahan and colleagues (Monahan and Muircheartaigh, 1980; Monahan et al., 1982) described the generation of sea salt particles from bursting bubbles. They fitted a power-law-shaped whitecap coverage function to the wind speed in 10 m height (Eq. (4)) (Monahan and Muircheartaigh, 1980). A sea salt particle number flux distribution was estimated for 100 % whitecap coverage and multiplied by the white cap coverage W (Monahan et al., 1986). The resulting parameterization Eq. (5) is valid on the size range $0.8\,\mu\text{m} < r_{80} < 20\,\mu\text{m}$.

$$W = 3.84 \times 10^{-6} \times u_{10}^{3.41} \tag{4}$$

$$\frac{dF_{\text{MO86}}}{dr_{80}} = W \times 3.576 \times 10^{5} \times r_{80}^{-3} \times 10^{1.19 \times e^{-B^2}} = 1.373 \times u_{10}^{3.41} \times r_{80}^{-3} \times 10^{1.19 \times e^{-B^2}} \tag{5}$$

$$B = \frac{0.380 - \log_{10}(r_{80})}{0.650}$$

Gong (2003) updated Monahan et al. (1986) for smaller size ranges given by Eq. (B1). The parameterization is valid on the size range $0.07\,\mu\text{m} < r_{80} < 20\,\mu\text{m}$. An adjustable dimensionless parameter θ was introduced and set to 30. However, a sensitivity study compared with observational data showed (Gantt et al., 2015) that setting θ to 8 improves Na^+ and $\text{PM}_{2.5}$ concentrations modeled with CMAQ. Hence in CMAQ v5.1, θ will be set accordingly.

Smith et al. (1993) fitted two log normal distributions given by Eq. (B3) to coarse sea salt particle measurements of $0.09\,\mu\text{m} < r_{\text{RH}} < 23.5\,\mu\text{m}$ performed on an island located 100 km off the north-west coast of the Scottish mainland. It was assumed that the relative humidity RH was approximately 80 % and that, based on preparation studies, surf zone emissions did not have a relevant contribution to the measured sea salt particles. Spada et al. (2013) considers the parameterization to be valid on the size range of $5\,\mu\text{m} < r_{80} < 30\,\mu\text{m}$.

Mårtensson et al. (2003) performed laboratory studies on SST (sea surface temperature) and salinity dependence of sea salt emissions. They derived a SST dependent particle number flux parameterization based on two polynomial fits of the degree 4 Eq. (B4). The whitecap coverage parameterization from Monahan and Muircheartaigh (1980) was employed (Eq. (4)). The polynomial coefficients (c_i and d_i) are given in Table S.1. Three sets of coefficients exist for three different intervals of Ddry. This parameterization is valid on the size range of $0.02\,\mu\text{m} < D_{\text{dry}} < 2.8\,\mu\text{m}$ and on the temperature range of $271\,\text{K} < SST < 298\,\text{K}$. However, the polynomial is negative for some D_{dry} when the third set of coefficients is used and $SST < 275.6\,\text{K}$. This situation needs special treatment when implemented.

Spada et al. (2013) compared several source functions and combinations of them on a global scale: They considered an extension of GO03 by SST (Jaeglé et al., 2011) and MA03/MO86/SM93 (Mårtensson et al., 2003; Monahan et al., 1986; Smith et al., 1993). The latter one is used in this study and abbreviated as SP13 Eq. (B5). Because of Eq. (2), we do not need to rewrite Eqs. (B1) and (B3). SP13 is valid on the size range $0.02\,\mu\text{m} < D_{\text{dry}} < 30\,\mu\text{m}$.

S.2.1 OV14

Recently, Ovadnevaite et al. (2014) published a new parameterization depending on wave state, wind speed and sea water viscosity ν_W whereby the viscosity depends on salinity (SAL) and SST Eq. (B6). The formula can be transformed to Eq. (6) by using Eq. (3) to facilitate the numeric integration.

$$\frac{dF_{\text{OV14}}}{dD_{\text{dry}}} = \ln 10 \times D_{\text{dry}} \times \sum_{i=1}^{5} \frac{F_i(\text{Re}_{\text{Hw}})}{\sqrt{2\pi} \times \log_{10}\sigma_i} \exp\left(-\frac{\log_{10}\frac{D_{\text{dry}}}{\text{GMD}_i}}{2 \times \log_{10}\sigma_i}\right) \tag{6}$$

$$\text{Re}_{\text{Hw}} = \frac{u_* \times H_S}{\nu_W} = \frac{\sqrt{C_D} \times u_{10} \times H_S}{\nu_W} \tag{7}$$

The factors GMD_i and σ_i and the functions $F_i(\text{Re}_{\text{Hw}})$ are given in Table S.2. The kinetic viscosity ν_W is calculated according to Eqs. (22) and (8) in Sharqawy et al. (2010). The source function is valid for a diameter size range of $0.015\,\mu\text{m} < D_{\text{dry}} < 6\,\mu\text{m}$.

In this study, the drag coefficient C_D was taken from WAM model runs of the coastDatII database (inside the North Sea) or was calculated according to Wu (1982) given in Eq. (8) (oceanic regions other than the North Sea). The friction velocity u_* is calculated from C_D by

Table S.1. Constants for Eq. B4. Values are taken from Mårtensson et al. (2003, Table 1) but given with more significant digits (Mårtensson, 2015, personal communication).

D_{dry} interval [µm]	c_4	c_3	c_2	c_1	c_0
0.020–0.145	−2.576 165 5e35	5.932 443 6e28	−2.867 174 3e21	−3.002 983 7e13	−2.880 813 5e6
0.145–0.419	−2.452 289 3e33	2.403 544 1e27	−8.147 834 1e20	1.182 850 3e14	−6.742 993 9e6
0.419–2.800	1.085 156 1e29	−9.841 434e23	3.132 359 3e18	−4.164 532 6e12	2.180 637 4e6

D_{dry} interval [µm]	d_4	d_3	d_2	d_1	d_0
0.020–0.145	7.188 465 6e37	−1.615 664 7e31	6.791 329 9e23	1.828 946 9e16	7.609 268 1e8
0.145–0.419	7.368 315 0e35	−7.310 214 9e29	2.528 340 4e23	−3.787 272 9e16	2.279 400 5e9
0.419–2.800	−2.859 476 2e31	2.601 213 7e26	−8.297 464 4e20	1.104 667 8e15	−5.800 388 0e8

Table S.2. Values for Eqs. (B6) and (6) but given with more significant digits than in the original parameterization (Ovadnevaite, 2015, personal communication). When one wants to reconstruct Fig. 4 in Ovadnevaite et al. (2014), one gets slight deviations due to rounding.

Mode (i)	GMD_i [µm]	σ_i [µm]	$F_i\,(\text{Re}_{\text{Hw}})$
1	0.018	1.37	$104.51 \times \left(\text{Re}_{\text{Hw}} - 10^5\right)^{0.556}$
2	0.041	1.5	$0.044 \times \left(\text{Re}_{\text{Hw}} - 10^5\right)^{1.08}$
3	0.09	1.42	$149.64 \times \left(\text{Re}_{\text{Hw}} - 10^5\right)^{0.545}$
4	0.23	1.53	$2.96 \times \left(\text{Re}_{\text{Hw}} - 10^5\right)^{0.79}$
5	0.83	1.85	$0.52 \times \left(\text{Re}_{\text{Hw}} - 2 \times 10^5\right)^{0.87}$

$$C_D = \begin{cases} 1.2875 \times 10^{-3}, & u_{10} < 7.5\,\frac{\text{m}}{\text{s}} \\ \left(0.8 + 0.065\,\frac{\text{s}}{\text{m}} \times u_{10}\right) \times 10^{-3}, & u_{10} \geq 7.5\,\frac{\text{m}}{\text{s}} \end{cases} \quad (8)$$

$$u_* = u_{10} \times \sqrt{C_D} \quad (9)$$

S.3 Surf Zone Treatment

The surf zone is implemented in accordance with Kelly et al. (2010) by setting the whitecap coverage to 1 within it. For each grid cell, the fraction of open ocean and surf zone is calculated in accordance with Neumann et al. (2016) and denoted as OPEN and SURF, respectively. In Eqs. (5), (B1), and (B4) the W is replaced by Eq. (10).

$$(W \times \text{OPEN} + \text{SURF}) \times \frac{1}{W} \quad (10)$$

Exemplary, applying this to GO03 Eq. (B1) leads to Eq. (11).

$$\begin{aligned} \frac{dF_{\text{GO03,net}}}{dr_{80}} &= (W \times \text{OPEN} + \text{SURF}) \times \frac{1}{W} \times \frac{dF_{\text{GO03}}}{dr_{80}} \quad (11) \\ &= (W \times \text{OPEN} + \text{SURF}) \times 3.576 \\ &\quad \times 10^5 r_{80}^{-A} \left(1 + 0.057 \times r_{80}^{3.45}\right) \times 10^{1.607 e^{-B^2}} \end{aligned}$$

S.4 Salinity Dependence

For this study, the GO03 and SP13 parameterizations were enhanced by a salinity dependence. Figure S.1 shows the dependence for three exemplary salinities. We assumed that the sea salt emission parameterizations were derived for a sea surface salinity of 35 ‰.

S.4.1 GO03

The sea salt number, surface area and mass (or volume) emissions are all scaled by the salinity SAL:

$$\frac{dF_{\text{GO03,net}}}{dr_{80}} = \frac{\text{SAL}}{35‰} \times (W \times \text{OPEN} + \text{SURF}) \times \frac{1}{W} \times \frac{dF_{\text{GO03}}}{dr_{80}} \quad (12)$$

Because GO03 sea salt emissions are calculated within CMAQ, one solution for implementing the salinity dependence was to modify CMAQ code. Because OPEN and SURF are read in externally from the OCEANfile (see Supplement of Neumann et al. (2016)), one can rewrite Eqs. (12) and (12) and scale OCEAN and SURF with SAL/35 ‰. Thus, no modifications in CMAQ are necessary.

$$\begin{aligned} \frac{dF_{\text{GO03,net}}}{dr_{80}} &= \left(W \times \frac{\text{SAL}}{35‰} \times \text{OPEN} + \frac{\text{SAL}}{35‰} \times \text{SURF}\right) \\ &\quad \times \frac{1}{W} \times \frac{dF_{\text{GO03}}}{dr_{80}} \quad (13) \end{aligned}$$

This approach was chosen in this study. OPEN and SURF are considered to be constant in time. This approach does not allow including annual or diurnal variations of the salinity dependence.

S.4.2 SP13

We assume that (a) inorganic ions are homogeneously distributed in the water column (no enrichment at the sea surface or in deeper water layers) and that (b) the water droplet generation process is not affected by variable salinity. Then sea surface salinity and gross dry sea salt mass emissions are proportional to each other because the droplet emission distribution does not change but the sea salt concentration within them does change. Further we assume that we can

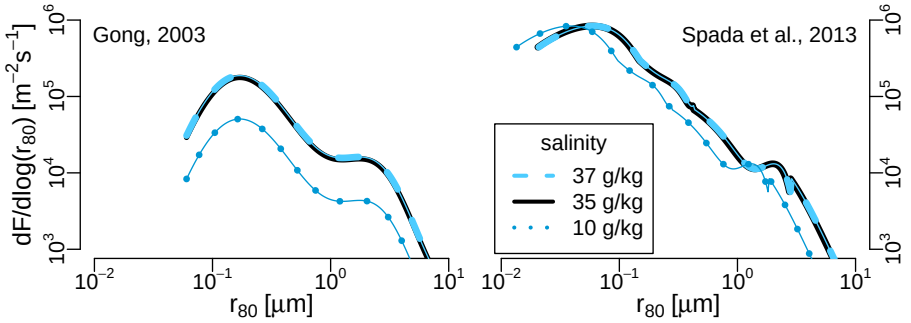

Figure S.1. Salinity dependence of the GO03 (left) and SP13 (right) parameterizations as implemented in this study. Parameters are chosen according to Figs. 2 and 3 in the main manuscript: $u_{10} = 8\,\mathrm{m\,s^{-1}}$, SST$= 283\,\mathrm{K}$, $C_D = 2.15 \times 10^{-3}$, $H_S = 1.23\,\mathrm{m}$, and $\nu_\mathrm{W} = 1.34 \times 10^{-6}\,\mathrm{m\,s^{-1}}$.

apply the same relation to net sea salt emissions. This assumption is not completely correct. Thus, in a region with 17.5 ‰ salinity, the dry sea salt mass emissions should be half as high compared with the emissions in a region with 35 ‰ salinity. The sea salt number emissions should remain unchanged but the dry mass of sea salt per individual sea salt particle $m_{\mathrm{dry,SAL}}$ should vary as described:

$$m_{\mathrm{dry,SAL}} = \frac{\mathrm{SAL}}{35‰} \times m_{\mathrm{dry},35‰} \tag{14}$$

Dry sea salt particle volume and dry sea salt particle mass are proportional to each other. Therefore, for the volume (V), surface area (A), and diameter (D) of individual sea salt particles follows:

$$V_{\mathrm{dry,SAL}} = \frac{\mathrm{SAL}}{35‰} \times V_{\mathrm{dry},35‰} \tag{15}$$

$$A_{\mathrm{dry,SAL}} = \left(\frac{\mathrm{SAL}}{35‰}\right)^{2/3} \times A_{\mathrm{dry},35‰} \tag{16}$$

$$D_{\mathrm{dry,SAL}} = \left(\frac{\mathrm{SAL}}{35‰}\right)^{1/3} \times D_{\mathrm{dry},35‰} \tag{17}$$

If Eq. (17) is applied to the particle emission size distribution in Eq. (B5) then the particle diameter needs to be scaled accordingly yielding a shift of the distribution by $\left(\sqrt[3]{\mathrm{SAL}/35‰} - 1\right) \times D_{\mathrm{dry}}$ to the right. If SAL $< 35‰$ then the shift is performed to the left (Figure S.1).

S.5 Integrating SP13 and OV14

The two sea salt source functions SP13 (Eqs. (B5) and (20)) and OV14 (Eq. (6)) were integrated as described in Sect. 2.2.3, in Table S.3, and in Fig. 3. Equation (20) shows how the salinity dependence described in Sect. S.4 is applied to Eq. (B5).

The water content of wet sea salt – compared to dry – was calculate in accordance with Lewis and Schwartz (2004, p.54) (or Lewis and Schwartz (2006) for exactly this formulation):

$$\frac{D_\mathrm{RH}}{D_{80}} = 0.54 \times \left(\frac{2 - \mathrm{RH}}{1 - \mathrm{RH}}\right)^{\frac{1}{3}} \tag{18}$$

Table S.3. Overview of the integration of SP13 and OV14. This table should be considered in combination with Fig. 3 in the main manuscript. $D_{\mathrm{dry,min,SAL}}$ and $D_{\mathrm{dry,max,SAL}}$ denote the minimum and maximum diameters, respectively, for those the SP13 parameterization is defined (see Sect. S.4.2). $D_{\mathrm{dry,Aa}}$ and $D_{\mathrm{dry,ac}}$ are the integration boundaries between the Aitken and accumulation mode (index **Aa**) and between the accumulation and coarse mode (index **ac**), respectively.

Size mode	SP13	OV14
Aitken	Whole function integrated from $D_{\mathrm{dry,min,SAL}}$ [a] to $D_{\mathrm{dry,Aa}}$ (= 0.1 µm)	Modes 1 and 2 integrated from 0.015 µm to 6 µm
accumulation	Whole function integrated from $D_{\mathrm{dry,Aa}}$ to $D_{\mathrm{dry,ac}}$ [b]	Modes 3 and 4 integrated from 0.015 µm to 6 µm
coarse	Whole function integrated from $D_{\mathrm{dry,ac}}$ [b] to $D_{\mathrm{dry,max,SAL}}$ [a]	Mode 5 integrated from 0.015 µm to 6 µm

[a] see Sect. S.5.1; [b] see Table S.4 for appropriate values

S.5.1 Integration boundaries for SP13

Values for the integration boundaries $D_{\mathrm{dry,min,SAL}}$, $D_{\mathrm{dry,Aa}}$, $D_{\mathrm{dry,ac}}$, and $D_{\mathrm{dry,max,SAL}}$ are needed for calculating Aitken, accumulation, and coarse mode emissions of the SP13 parameterization. The values for $D_{\mathrm{dry,min,SAL}}$ and $D_{\mathrm{dry,max,SAL}}$ are derived from the definition range of the parameterization and the value for $D_{\mathrm{dry,Aa}}$ is given in Table 18. The integration boundary between accumulation and coarse mode ($D_{\mathrm{dry,ac}}$) is not defined yet. It was set equal to the intersection between accumulation and coarse mode distributions of the GO03 sea salt emission parameterizations as implemented in CMAQ: Both modal distributions are discrete functions of RH. For this study, the intersection wet diameter was calculated for each discrete RH value and converted into the corresponding dry diameter (Table S.4). The resulting dry diameter depends

on RH which is an artifact. However, this dependency was kept in order to be consistent with CMAQ sea salt emissions.

Table S.4. RH dependent integration boundary between accumulation and coarse mode as dry diameter $D_{\text{dry,ac}}$ for integrating the SP13 parameterization.

RH [%]	$D_{\text{dry,ac}}$ [µm]	RH [%]	$D_{\text{dry,ac}}$ [µm]
45	1.276076	…	…
50	1.324269	80	1.498309
55	1.347672	85	1.49023
60	1.388263	90	1.514228
65	1.415549	93	1.550082
70	1.45391	95	1.578587
75	1.479312	97	1.577349
…	…	99	1.361808

Including salinity dependence into the integration of SP13 is not straightforward. Therefore, it is described in detail. We define a function f_{sp}

$$f_{sp}(D_{\text{dry}}) = \frac{dF_{\text{SP13}}}{dD_{\text{dry}}} \tag{19}$$

in order to express the salinity dependence mathematically by

$$\begin{aligned}\frac{dF_{\text{SP13,SAL}}}{dD_{\text{dry}}} &= f_{\text{sp, SAL}}(D_{\text{dry}}) \\ &= f_{\text{sp}}\left(D_{\text{dry}} \times \left(\frac{35‰}{\text{SAL}}\right)^{1/3}\right)\end{aligned} \tag{20}$$

The salinity dependent source function as defined by Eq. (20) is not valid on the same interval as Eq. (B5) anymore; that was

$$D_{\text{dry,min}} = 0.02\,\mu\text{m} < D_{\text{dry}} < 30\,\mu\text{m} = D_{\text{dry,max}}$$

But rather it is valid on the interval

$$\begin{aligned}D_{\text{dry,min,SAL}} &= 0.02\,\mu\text{m} \times \left(\frac{\text{SAL}}{35‰}\right)^{1/3} \\ &< D_{\text{dry}} \\ &< 30\,\mu\text{m} \times \left(\frac{\text{SAL}}{35‰}\right)^{1/3} = D_{\text{dry,max,SAL}}\end{aligned}$$

Further, we define that the boundaries between Aitken and accumulation mode ($D_{\text{dry,Aa}}$) and between accumulation and coarse mode ($D_{\text{dry,ac}}$) remain unaffected by changes in the salinity. $D_{\text{dry,ac}}$ depends on RH (Table S.4).

$$\begin{aligned}D_{\text{dry,Aa}} &= 0.1\,\mu\text{m} \\ D_{\text{dry,ac}} &= D_{\text{dry,ac}}(\text{RH})\end{aligned}$$

The dry sea salt number, surface area, and volume emissions are integrated based on these definitions and assumptions (Table S.5). Dry mass emissions are calculated from the volume emissions by multiplication with $\rho_{\text{sea salt}}$ which is considered to be $2.2\,\text{g}\,\text{cm}^{-3}$.

S.6 Input Data

Figure S.2 shows the regions that are covered by different sets of input data. The COSMO-CLM meteorological data set covers the whole study region and is not marked in the map. ERA-Interim wave and ocean data were used outside of the blue and orange colored regions except for the salinity. The latter was set to 35 ‰ in the Atlantic Ocean, 37 ‰ in the Mediterranean Sea, and 18 ‰ in the Black Sea. Table S.6 shows the source and resolution of the input data that were used for calculation sea salt emissions for the five sea regions – North Sea, Baltic Sea, Atlantic Ocean, Mediterranean Sea, and Black Sea.

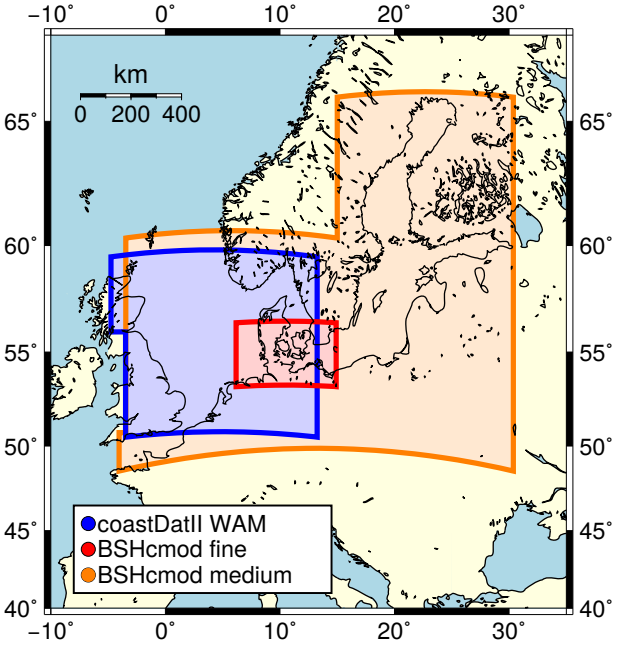

Figure S.2. Map showing the locations corresponding to the input data from each source. **Wave data:** In the blue region, wave data from coastDatII were used. Outside this region, the significant wave height data were acquired from ERA-Interim and the friction velocity data were calculated based on meteorological input data. **SST and SAL data:** In the orange and red regions, SST and SAL data were acquired from BSHcmod with medium and fine grid resolutions, respectively. Outside the orange region, the SST data were acquired from ERA-Interim and the salinity was set to a fixed value (see text). **Meteorological data:** The same meteorological data were used for the entire map region.

Table S.5. Integrals for calculating salinity dependent SP13 sea salt emissions.

	Number Emissions	Surface area Emissions	Volume Emissions
Aitken	$\int_{D_{\text{min}}}^{D_{\text{Aa}}} f_{\text{sp}}\left(\frac{D}{\sqrt[3]{\frac{S}{35‰}}}\right)\mathrm{d}D$	$\int_{D_{\text{min}}}^{D_{\text{Aa}}} \pi D^2 \times f_{sp}\left(\frac{D}{\sqrt[3]{\frac{S}{35‰}}}\right)\mathrm{d}D$	$\int_{D_{\text{min}}}^{D_{\text{Aa}}} \frac{\pi}{6} D^3 \times f_{sp}\left(\frac{D}{\sqrt[3]{\frac{S}{35‰}}}\right)\mathrm{d}D$
acc.	$\int_{D_{\text{Aa}}}^{D_{ac}} f_{sp}\left(\frac{D}{\sqrt[3]{\frac{S}{35‰}}}\right)\mathrm{d}D$	$\int_{D_{\text{Aa}}}^{D_{ac}} \pi D^2 \times f_{sp}\left(\frac{D}{\sqrt[3]{\frac{S}{35‰}}}\right)\mathrm{d}D$	$\int_{D_{\text{Aa}}}^{D_{ac}} \frac{\pi}{6} D^3 \times f_{sp}\left(\frac{D}{\sqrt[3]{\frac{S}{35‰}}}\right)\mathrm{d}D$
coarse	$\int_{D_{ac}}^{D_{\text{max}}\sqrt[3]{\frac{S}{35‰}}} f_{sp}\left(\frac{D}{\sqrt[3]{\frac{S}{35‰}}}\right)\mathrm{d}D$	$\int_{D_{ac}}^{D_{\text{max}}\sqrt[3]{\frac{S}{35‰}}} \pi D^2 \times f_{sp}\left(\frac{D}{\sqrt[3]{\frac{S}{35‰}}}\right)\mathrm{d}D$	$\int_{D_{ac}}^{D_{\text{max}}\sqrt[3]{\frac{S}{35‰}}} \frac{\pi}{6} D^3 \times f_{sp}\left(\frac{D}{\sqrt[3]{\frac{S}{35‰}}}\right)\mathrm{d}D$

S.7 Setup of CMAQ runs

The $24 \times 24\text{km}^2$ and $72 \times 72\text{km}^2$ grids are denoted as CD24 and CD72 grids (Fig. 1) and defined in the attached GRIDDESC file.

Six Ocean files are attached – three for each grid. The identifier _sf050m indicates that a surf zone of 50 m width is assumed. The identifier _sal indicates that the OPEN and SURF variables are scaled by the salinity as described in Sect. S.4.1. The identifier _noSalt indicates that OPEN and SURF are set to 0 (zero) so that no sea salt is emitted. The identifier _GIS_ubound indicates that the coastline data were extracted via ArcGIS and that the SURF variable has an upper bound as described in Supplement to Neumann et al. (2016), respectively. Table S.7 shows which Ocean file was used for each emission case.

S.8 Modifications in CMAQ

S.8.1 Changes in the CMAQ Code

The modules AERO_EMIS.F (minor changes) and SSEMIS.F were modified. All other modules were kept unchanged. The modified source code files are attached in the supplement. Modifications in the modules and subroutines/functions are documented in the beginning of each one by "[DATE] Neumann: ..." and indicated in the code by "NEUMANND". There are four types of comments indicating modifications:

1. new variables

```
! NEW VARIABLES BY NEUMANND
[VARIABLE DEFINITION]
```

2. long new code passages

```
! START NEUMANND
[CODE]
! END NEUMANND
```

3. individual new code lines

```
! NEW NEUMANND: [DESCRIPTION]
[CODE] ! NEW
```

4. individual modified code lines

```
! MODIFIED NEUMANND: [DESCRIPTION]
[CODE] !
```

S.8.2 Changes in the Namelist files

Commonly, sea salt emissions consist of accumulation and coarse mode emissions. The SP13 and OV14 parameterizations were implemented to emit Aitken, accumulation, and coarse mode sea salt particles. However, if Aitken mode sea salt emissions are considered, they should be displayed in the output files. For this purpose the aerosol namelist file (AE_cb05tucl_ae5_aq.nml) needs to be modified. In the line starting with ANAI, the columns DDEP, WDEP and CONC have to be set to Yes. Alternatively, one can replace the line

```
'ANAI:2 3 .0:ANAI:1 .0:VMASSI:1 .0:NA_AITKEN
    :1 .0:::NA_AITKEN:Yes:::',
```

by the line

```
'ANAI:2 3 .0:ANAI:1 .0:VMASSI:1 .0:NA_AITKEN
    :1 .0:::NA_AITKEN:Yes:Yes:Yes:Yes',
```

S.8.3 Additions in the CMAQ Run Script

Two new environment variables need to be set in the CMAQ run script in order to read in sea salt emissions externally. Below, a code example is given (Listing 1).

Listing 1. New variables which need to be added to the CMAQ start scripts when external sea salt emissions should be imported.

```
#> read sea-salt emissions from
#    external file [ N|F ]
```

Table S.6. Overview of the input data used for calculating sea salt emissions.

Parameter	Resolution	Region	Model [Database]	Reference
Meteorology	$0.22° \times 0.22°$ lon x lat, rotated	Whole model domain	COSMO-CLM v4.8 [coastDatII]	Geyer and Rockel (2013) Geyer (2014)
Waves (H_S, C_D)	$0.075° \times 0.05°$ lon $\times$ lat	North Sea (southward of $59.2°$ N and eastward of $4.75°$ W)	WAM 4.5.3 [coastDatII]	Groll et al. (2014)
Waves (H_S)	$1° \times 1°$	Atlantic Ocean, Baltic Sea, Mediterranean Sea, Black Sea	WAM [ERA-Interim]	Dee et al. (2011)
Waves (C_D)	see Meteorology	Atlantic Ocean, Baltic Sea, Mediterranean Sea, Black Sea	derived from u_{10} [coastDatII]	Wu (1982)
SST, SAL	$5' \times 3'$ lon $\times$ lat	North and Baltic Sea	BSHcmod4, coarse grid	Dick et al. (2001), BSH[a]
SST, SAL	$50'' \times 30''$ lon $\times$ lat	German waters in North and Baltic Sea	BSHcmod4, fine grid	Dick et al. (2001), BSH[a]
SST	$1° \times 1°$	Atlantic Ocean, Mediterranean Sea, Black Sea	ERA input only [ERA-Interim, NCEP]	
SAL	–	Atlantic Ocean, Mediterranean Sea, Black Sea	Atlantic: $35‰$, Med. Sea: $37‰$, Black Sea: $18‰$	

[a] www.bsh.de/en/Marine_data/Forecasts/Prediction_models/index.jsp

Table S.7. Usage of the three Ocean files in the four sea salt emission cases. The asterisks replace CD24 and CD72.

Case	Ocean files
zero	OCEAN_*_noSalt_GIS.nc
GO03	OCEAN_*_sf050m_GIS_ubound_sal.nc
SP13	OCEAN_*_sf050m_GIS_ubound.nc
OV14	OCEAN_*_sf050m_GIS_ubound.nc

```
setenv CTM_READSSEMIS Y

#> Sea Salt emissions
# example file name
set SS_FILE = SSEMIS.${STDATE}
# example directory name
set SS_DIR  = /example/ssemis

#> file containing the sea-salt
#    emissions
setenv SSEMIS_1 ${SS_DIR}/${SS_FILE}
```

S.9 Emissions

The Figs. S.3 to S.5 show sea salt mass, surface area, and number emissions, respectively, at one location in the German Bight. Figure S.6 shows the GMD of the emissions at the same locations. In each figure, Aitken-, accumulation- and coarse-mode emissions are plotted (top to bottom). The plots show winter (left) and summer emissions (right).

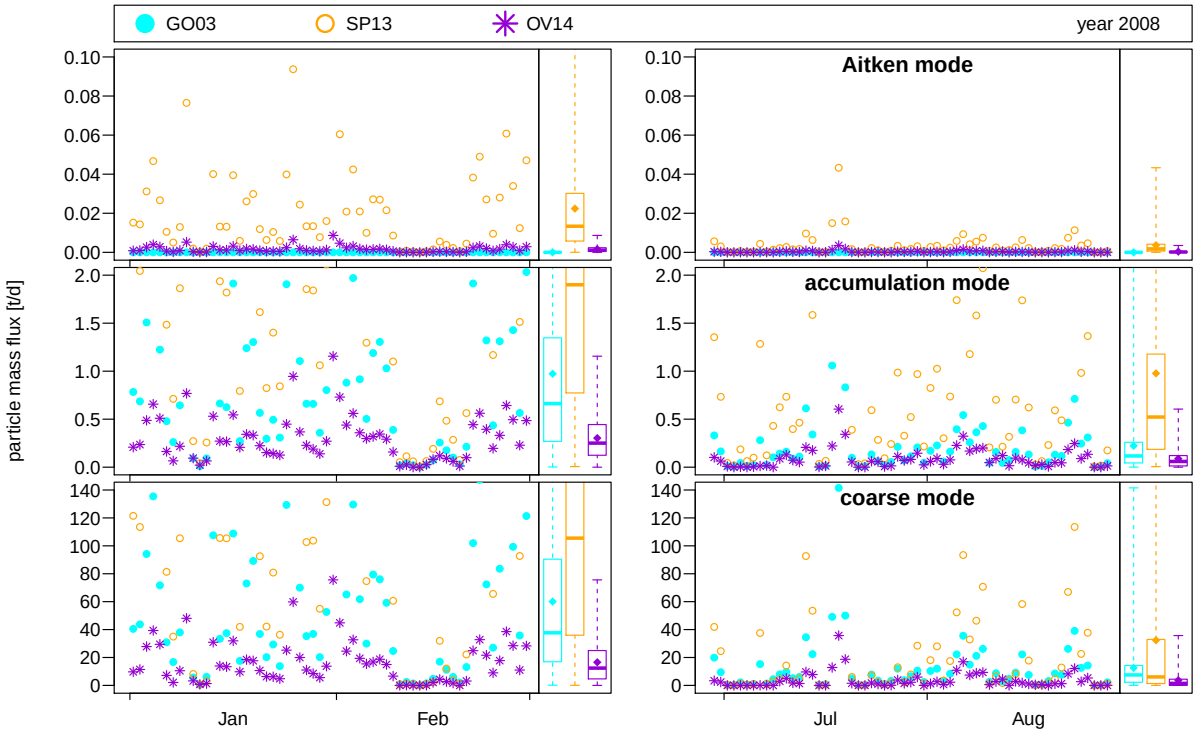

Figure S.3. Sea salt mass emissions [$\mathrm{t\,d^{-1}}$] into the Aitken, accumulation, and coarse modes (top to bottom) at one location in the German Bight in winter (left) and summer (right) 2008.

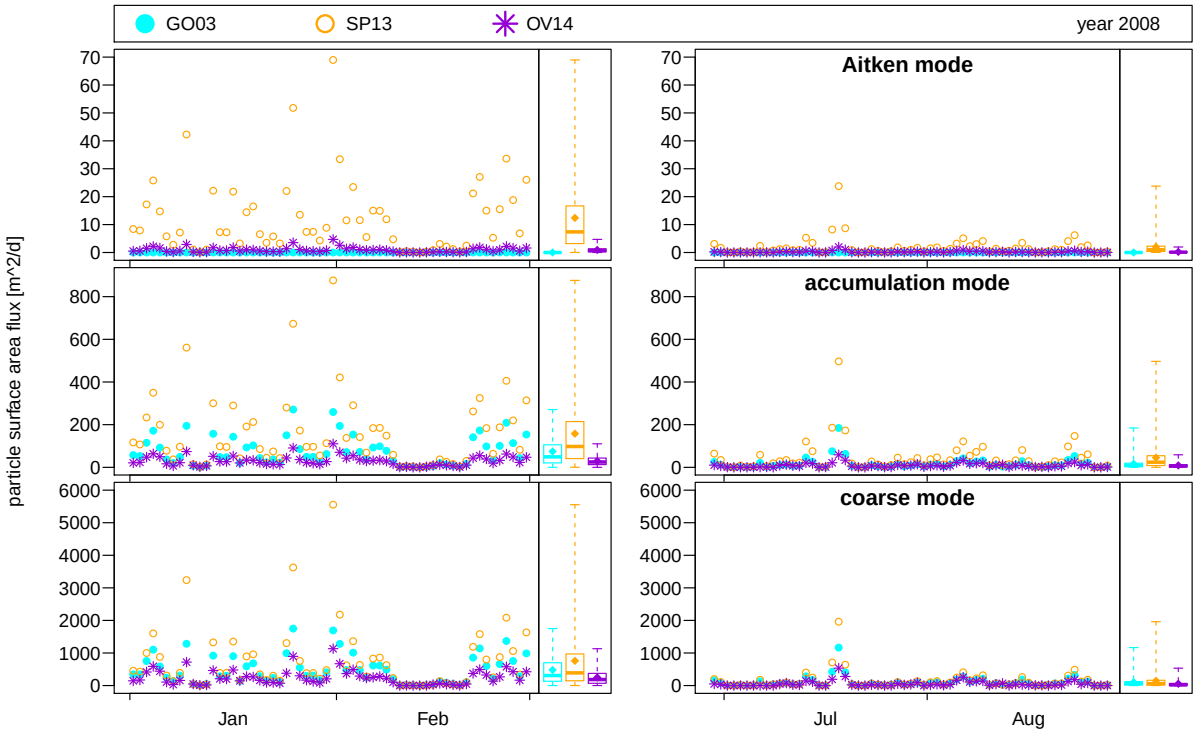

Figure S.4. Similar to Fig. S.3 but showing sea salt particle surface area emissions [$\mathrm{m^2\,d^{-1}}$].

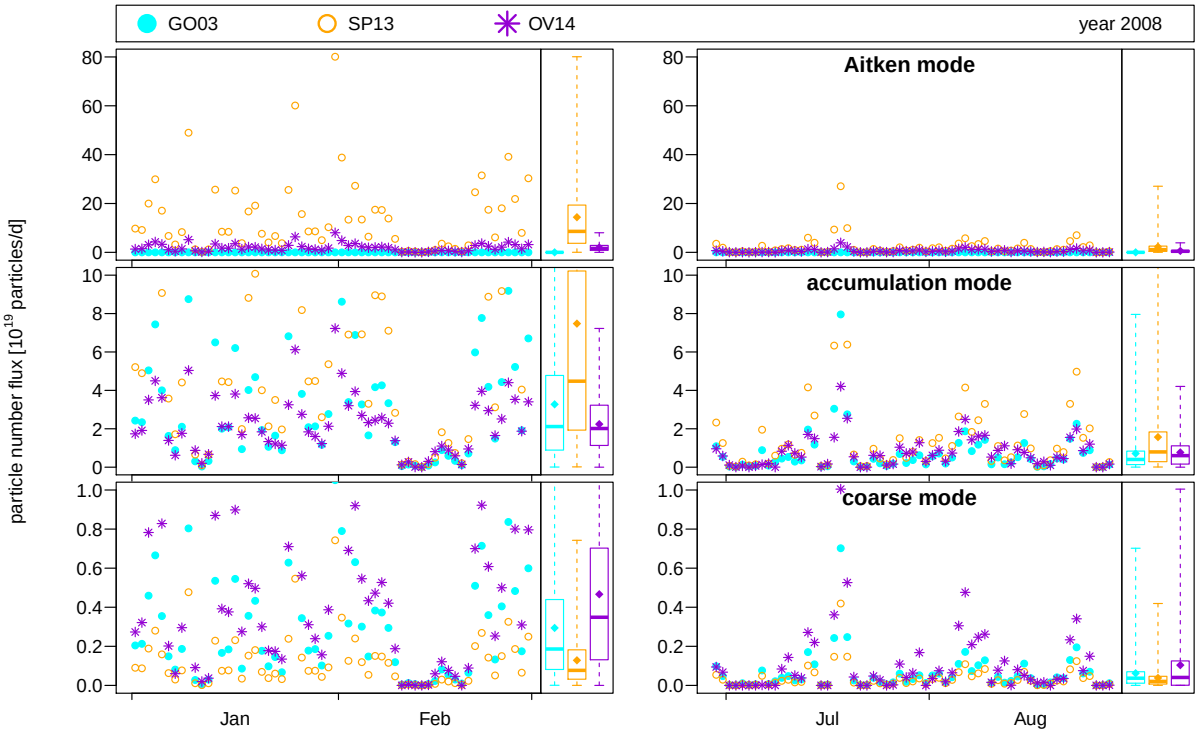

Figure S.5. Similar to Fig. S.3 but showing sea salt particle number emissions [1×10^{19} particles d^{-1}].

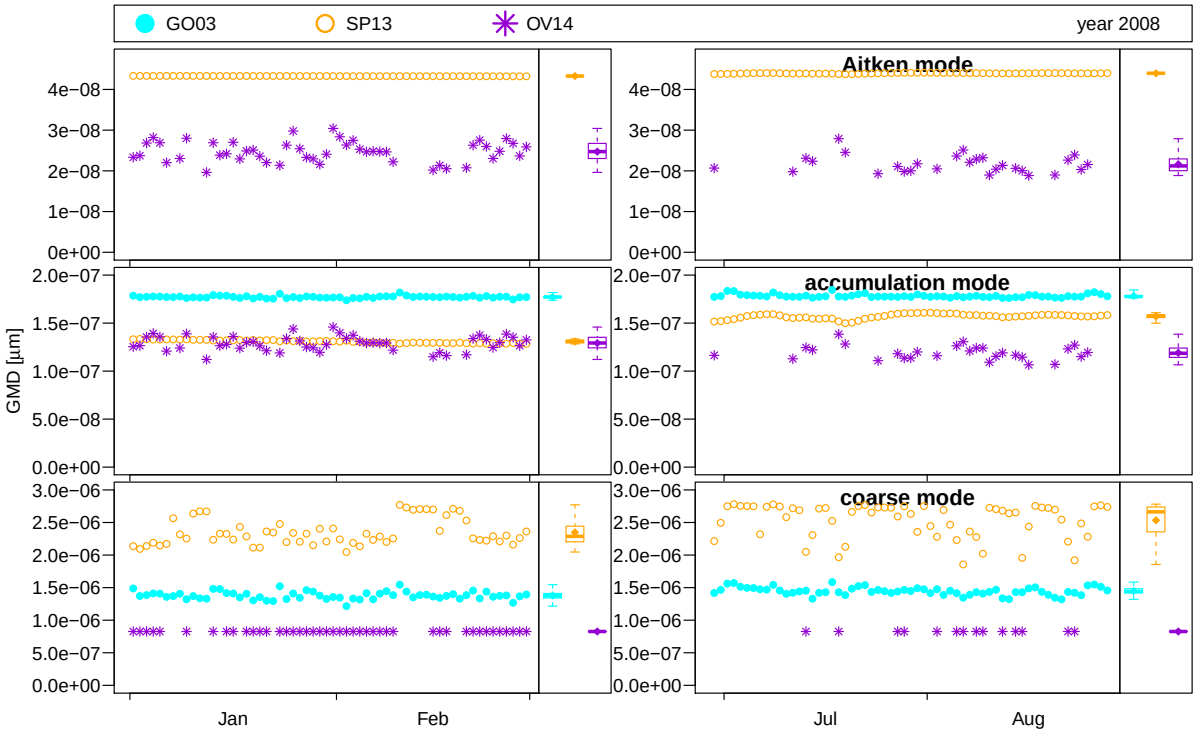

Figure S.6. Similar to Fig. S.3 but showing the GMDs of the emitted sea salt particle Aitken, accumulation and coarse mode distributions (top to bottom). Log-normal distributed modes are assumed in order to calculate the GMD (Binkowski and Roselle, 2003). As Fig. 2 shows, this assumption is not justified. However, log-normal shaped emissions and concentrations are assumed in CMAQ.

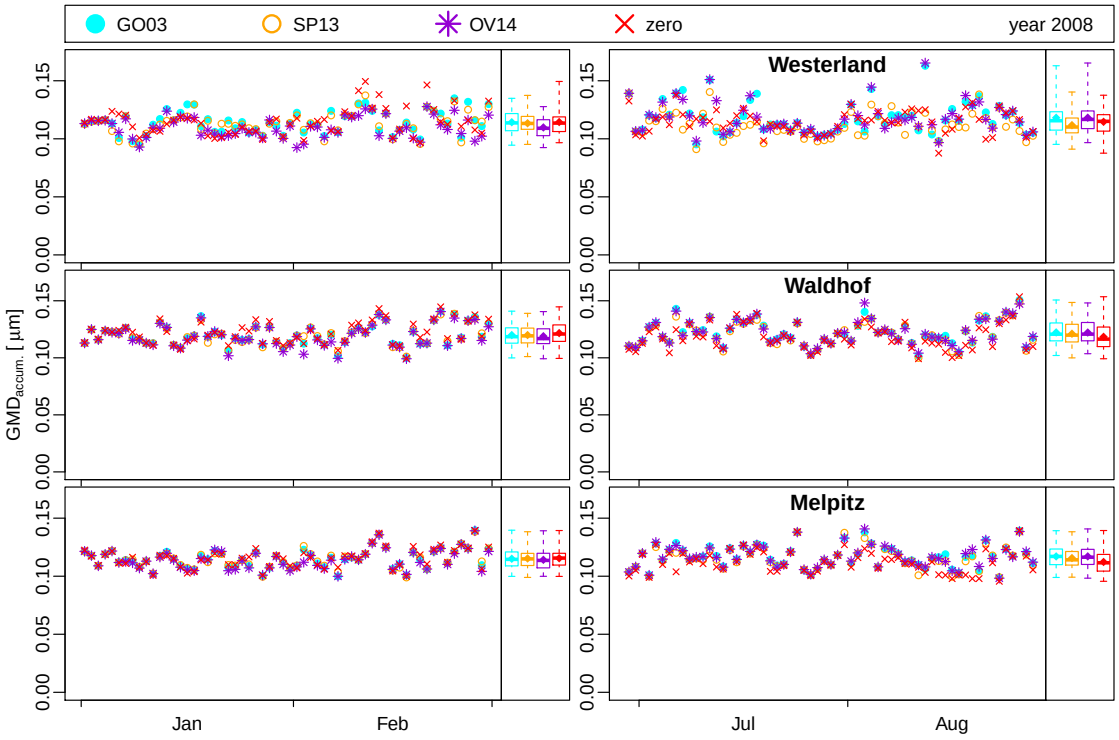

Figure S.7. Geometric mean diameter (GMD) of the accumulation mode of the GO03, SP13, OV14, and zero emission cases at the stations Westerland, Waldhof, and Melpitz (top to bottom) in winter and summer (left to right).

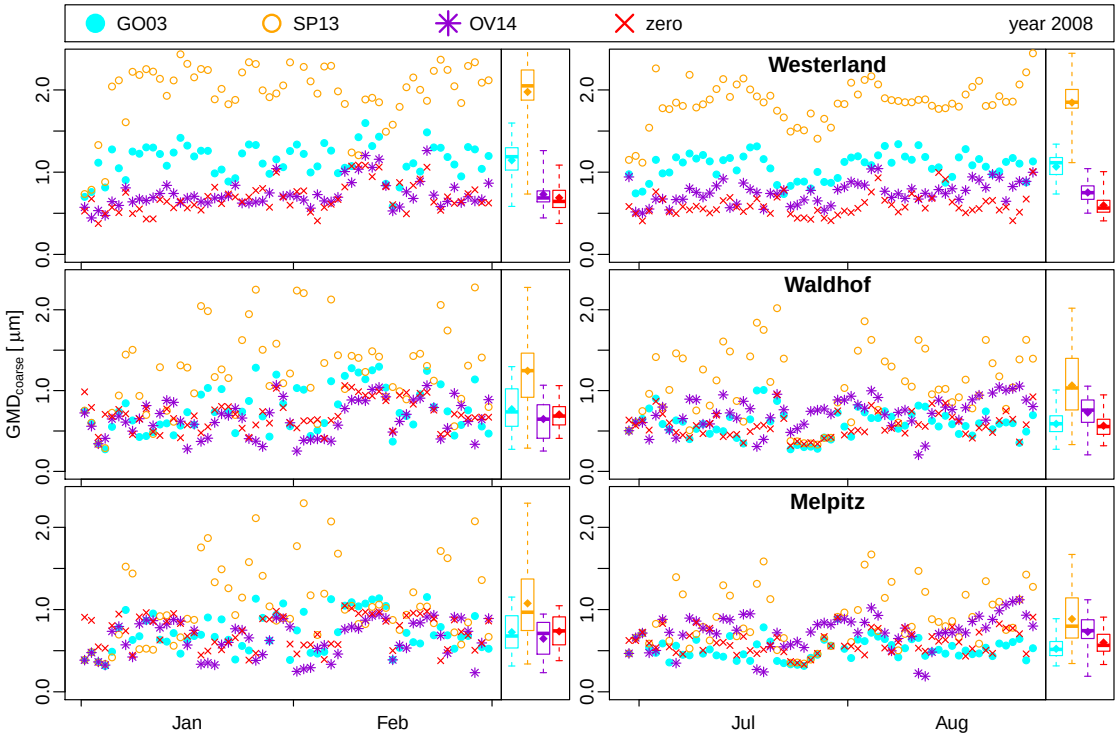

Figure S.8. Similar to Fig. S.7 but coarse-mode GMDs.

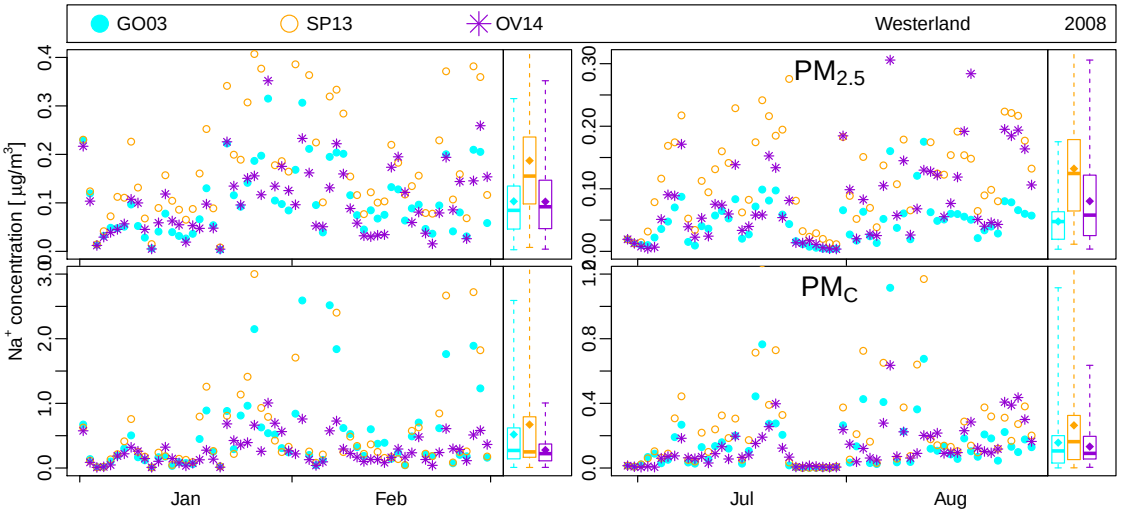

Figure S.9. Similar to Fig. 12 but showing data for Waldhof.

Table S.8. Similar to Table 5 but showing precipitation in mm.

precipitation	Winter 2008					Summer 2008				
Station	n	RAE	R	μ_P	μ_O	n	RAE	R	μ_P	μ_O
Råö	38	1.464	0.753	3.474	3.403	26	7.675	0.207	6.561	7.262
Leba	31	2.292	0.304	2.064	2.016	28	4.485	0.634	3.840	6.214
Preila	20	4.726	0.230	2.939	2.030	29	7.846	-0.105	3.786	5.414
Rucava	18	5.466	0.156	3.905	5.067	30	5.954	0.329	3.170	7.530
Birkenes	37	8.438	0.571	6.211	13.941	27	10.949	0.538	6.844	13.604
Kårvatn	31	10.048	0.094	0.646	10.606	24	11.179	-0.187	7.710	8.871
Tustervatn	36	7.136	0.183	0.645	6.886	22	4.488	0.029	5.286	4.277
Waldhof	19	2.748	0.762	5.338	5.237	30	4.590	0.475	2.473	6.123
Neuglobsow	22	3.228	0.399	3.772	4.264	22	5.407	0.292	2.493	5.636
Zoseni	12	7.404	0.252	1.554	5.833	29	5.937	0.184	1.944	7.072
Diabla Gora	21	3.520	0.562	2.501	3.676	25	6.941	0.324	1.919	7.060
Løken	32	4.470	0.488	1.972	5.678	25	10.752	0.142	5.084	11.652
Hurdal	26	8.612	0.461	0.116	8.685	28	8.220	0.592	4.515	8.839
Jarczew	24	2.008	0.661	2.671	3.479	17	7.399	-0.158	1.559	7.512

S.10 Atmospheric Data

The accumulation and coarse mode GMDs at the stations Westerland, Waldhof, and Melpitz are briefly mentioned in the manuscript. Figures S.7 and S.8 present the GMDs at these stations. As extension to Figs. 11 and 12 in the manuscript, Figure S.9 shows the sodium $PM_{2.5}$ and PM_C concentrations at the station of Waldhof, which is located spatially in between Westerland and Melpitz stations.

S.11 Precipitation

Table 5 in Sect. 3.3 of the manuscript presents the sodium wet deposition at 14 EMEP measurement stations. Table S.8 contains the corresponding precipitation amounts.

Table S.9. AERONET stations that were considered for the statistical evaluation. The column "Usage" indicates whether the data are shown in the manuscript (Table 6) or in the Supplement (Table S.10). Statistical data of the stations Helgoland (near Westerland) and Leipzig (close to Melpitz) are additionally plotted in Fig. 13.

Station Name	Usage	Lon	Lat	Height [m]	Location
Helgoland	Fig. 13, Table 6	7.887	54.178	33	Coast
Helsinki Lighthouse	Table S10	24.926	59.949	20	Coast
Oostende	Table S10	2.925	51.225	23	Coast
Dunkerque	Table S10	2.368	51.035	0	Coast
Cabauw	Table 6	4.927	51.971	-1	Coast
Lille	Table 6	3.142	50.612	60	Coast
Brussels	Table S10	4.35	50.783	120	Inland
Hamburg	Table S10	9.973	53.568	105	Inland
Palgrunden	Table S10	13.152	58.755	49	Inland
Toravere	Table S10	26.46	58.255	70	Inland
Gustav Dalen Tower	Table 6	17.467	58.594	25	Mixed
Hyytiala	Table S10	24.296	61.846	191	Inland
Mainz	Table 6	8.3	49.999	150	Inland
Leipzig	Fig. 13, Table 6	12.435	51.352	125	Inland
Kuopio	Table S10	27.634	62.892	105	Inland
Belsk	Table S10	20.792	51.837	190	Inland
Minsk	Table S10	27.601	53.92	200	Inland

S.12 Aerosol Optical Depth

Table S.9 lists all AERONET stations that were used for the statistical evaluation. The column "usage" indicates whether the measured data were plotted, shown in Table 6 of the manuscript or only plotted in Table S.10. The latter table shows the statistical metrics on all stations listed in Table S.9.

References

Dee, D. P., Uppala, S. M., Simmons, A. J., Berrisford, P., Poli, P., Kobayashi, S., Andrae, U., Balmaseda, M. A., Balsamo, G., Bauer, P., Bechtold, P., Beljaars, A. C. M., van de Berg, L., Bidlot, J., Bormann, N., Delsol, C., Dragani, R., Fuentes, M., Geer, A. J., Haimberger, L., Healy, S. B., Hersbach, H., Hólm, E. V., Isaksen, L., Kållberg, P., Köhler, M., Matricardi, M., McNally, A. P., Monge-Sanz, B. M., Morcrette, J.-J., Park, B.-K., Peubey, C., de Rosnay, P., Tavolato, C., Thépaut, J.-N., and Vitart, F.: The ERA-Interim reanalysis: configuration and performance of the data assimilation system, Q. J. Roy. Meteor. Soc., 137, 553–597, doi:10.1002/qj.828, http://dx.doi.org/10.1002/qj.828, 2011.

Dick, S., Mueller-Navarra, S., Klein, H., Komo, H., and Kleine, E.: The operational circulation model of BSH (BSHcmod) - model description and validation, Techreport, Bundesamt fuer Seeschiffahrt und Hydrographie, http://hdl.handle.net/10068/186797, 2001.

Gantt, B., Kelly, J. T., and Bash, J. O.: Updating sea spray aerosol emissions in the Community Multiscale Air Quality (CMAQ) model version 5.0.2, Geosci. Model Dev., 8, 3733–3746, doi:10.5194/gmd-8-3733-2015, http://www.geosci-model-dev.net/8/3733/2015/, 2015.

Geyer, B.: High-resolution atmospheric reconstruction for Europe 1948-2012: coastDat2, Earth Syst. Sci. Data, 6, 147–164, doi:10.5194/essd-6-147-2014, http://www.earth-syst-sci-data.net/6/147/2014/, 2014.

Geyer, B. and Rockel, B.: coastDat-2 COSMO-CLM Atmospheric Reconstruction, World Data Center for Climate (WDCC), Hamburg, Germany, doi:10.1594/WDCC/coastDat-2_COSMO-CLM, http://cera-www.dkrz.de/WDCC/ui/Compact.jsp?acronym=coastDat-2_COSMO-CLM, 2013.

Gong, S. L.: A parameterization of sea-salt aerosol source function for sub- and super-micron particles, Global Biogeochem. Cycles, 17, 1097, doi:10.1029/2003GB002079, http://dx.doi.org/10.1029/2003GB002079, 2003.

Groll, N., Grabemann, I., and Gaslikova, L.: North Sea wave conditions: an analysis of four transient future climate realizations, Ocean Dynam., 64, 1–12, doi:10.1007/s10236-013-0666-5, http://dx.doi.org/10.1007/s10236-013-0666-5, 2014.

Jaeglé, L., Quinn, P. K., Bates, T. S., Alexander, B., and Lin, J.-T.: Global distribution of sea salt aerosols: new constraints from in situ and remote sensing observations, Atmos. Chem. Phys., 11, 3137–3157, doi:10.5194/acp-11-3137-2011, http://www.atmos-chem-phys.net/11/3137/2011/, 2011.

Lewis, E. R. and Schwartz, S. E.: Sea Salt Aerosol Production: Mechanisms, Methods, Measurements and Models - A Critical Review, vol. 152, AGU, Washington, D. C., doi:10.1029/GM152, 2004.

Lewis, E. R. and Schwartz, S. E.: Comment on "size distribution of sea-salt emissions as a function of relative humidity", Atmos. Environ., 40, 588–590, doi:10.1016/j.atmosenv.2005.08.043, http://www.sciencedirect.com/science/article/pii/S1352231005009672, 2006.

Monahan, E. C. and Muircheartaigh, I. O.: Optimal Power-Law Description of Oceanic Whitecap Coverage Dependence on Wind

Table S.10. Similar to Table 6 but showing statistical figures of all stations listed in Table S.9 but missing in Table 6.

aerosol optical depth		Winter 2008				Summer 2008			
Station	Case	n	RAE	MNB	R	n	RAE	MNB	R
Helsinki Lighthouse	GO03	0	NaN	NaN	NA	129	0.02	0.13	0.25
Coast	SP13	0	NaN	NaN	NA	129	0.02	0.13	0.28
	OV14	0	NaN	NaN	NA	129	0.02	0.18	0.10
	ZERO	0	NaN	NaN	NA	129	0.02	0.06	0.24
Oostende	GO03	0	NaN	NaN	NA	105	0.08	0.09	0.19
Coast	SP13	0	NaN	NaN	NA	105	0.08	0.13	0.19
	OV14	0	NaN	NaN	NA	105	0.08	0.14	0.19
	ZERO	0	NaN	NaN	NA	105	0.09	0.08	0.17
Dunkerque	GO03	83	0.06	0.30	-0.03	51	0.07	-0.18	0.06
Coast	SP13	83	0.06	0.36	-0.06	51	0.07	-0.16	0.09
	OV14	83	0.06	0.32	-0.01	51	0.07	-0.16	0.09
	ZERO	83	0.06	0.31	0.01	51	0.07	-0.19	-0.01
Brussels	GO03	0	NaN	NaN	NA	56	0.09	-0.25	0.45
Inland	SP13	0	NaN	NaN	NA	56	0.09	-0.24	0.46
	OV14	0	NaN	NaN	NA	56	0.09	-0.24	0.46
	ZERO	0	NaN	NaN	NA	56	0.09	-0.26	0.46
Hamburg	GO03	0	NaN	NaN	NA	82	0.10	-0.39	-0.08
Inland	SP13	0	NaN	NaN	NA	82	0.10	-0.39	-0.08
	OV14	0	NaN	NaN	NA	82	0.10	-0.38	-0.10
	ZERO	0	NaN	NaN	NA	82	0.10	-0.42	-0.11
Palgrunden	GO03	0	NaN	NaN	NA	191	0.03	-0.25	0.11
Inland	SP13	0	NaN	NaN	NA	191	0.03	-0.22	0.11
	OV14	0	NaN	NaN	NA	191	0.03	-0.22	0.10
	ZERO	0	NaN	NaN	NA	191	0.03	-0.32	0.12
Toravere	GO03	2	0.04	-0.43	-1.00	101	0.05	-0.12	0.18
Inland	SP13	2	0.03	-0.31	1.00	101	0.05	-0.11	0.18
	OV14	2	0.04	-0.47	-1.00	101	0.05	-0.09	0.14
	ZERO	2	0.05	-0.64	-1.00	101	0.05	-0.18	0.18
Hyytiala	GO03	0	NaN	NaN	NA	81	0.04	-0.36	0.25
Inland	SP13	0	NaN	NaN	NA	81	0.04	-0.36	0.25
	OV14	0	NaN	NaN	NA	81	0.04	-0.33	0.27
	ZERO	0	NaN	NaN	NA	81	0.04	-0.39	0.14
Kuopio	GO03	0	NaN	NaN	NA	71	0.03	-0.42	0.54
Inland	SP13	0	NaN	NaN	NA	71	0.03	-0.42	0.51
	OV14	0	NaN	NaN	NA	71	0.03	-0.40	0.47
	ZERO	0	NaN	NaN	NA	71	0.03	-0.45	0.50
Belsk	GO03	22	0.11	-0.06	-0.44	204	0.06	-0.20	0.25
Inland	SP13	22	0.11	0.00	-0.45	204	0.06	-0.20	0.24
	OV14	22	0.11	-0.09	-0.44	204	0.06	-0.18	0.26
	ZERO	22	0.11	-0.13	-0.42	204	0.06	-0.23	0.22
Minsk	GO03	6	0.05	0.71	0.71	142	0.09	-0.45	0.43
Inland	SP13	6	0.05	0.76	0.71	142	0.09	-0.45	0.43
	OV14	6	0.05	0.68	0.71	142	0.09	-0.43	0.41
	ZERO	6	0.04	0.57	0.71	142	0.09	-0.48	0.44

Speed, J. Phys. Oceanogr., 10, 2094–2099, doi:10.1175/1520-0485(1980)010<2094:OPLDOO>2.0.CO;2, http://dx.doi.org/10.1175/1520-0485(1980)010<2094:OPLDOO>2.0.CO;2, 1980.

Monahan, E. C., Davidson, K. L., and Spiel, D. E.: Whitecap aerosol productivity deduced from simulation tank measurements, J. Geophys. Res. Oceans, 87, 8898–8904, doi:10.1029/JC087iC11p08898, http://dx.doi.org/10.1029/JC087iC11p08898, 1982.

Monahan, E. C., Spiel, D. E., and Davidson, K. L.: A Model of Marine Aerosol Generation via Whitecaps and Wave Disruption, pp. 167–174, Oceanographic Sciences Library, Springer, Dordrecht, Netherlands, doi:10.1007/978-94-009-4668-2_16, http://dx.doi.org/10.1007/978-94-009-4668-2_16, 1986.

Mårtensson, E. M.: personal communication, 2015.

Mårtensson, E. M., Nilsson, E. D., de Leeuw, G., Cohen, L. H., and Hansson, H.-C.: Laboratory simulations and parameterization of the primary marine aerosol production, J. Geophys. Res. Atmos., 108, 4297, doi:10.1029/2002JD002263, http://dx.doi.org/10.1029/2002JD002263, 2003.

Neumann, D., Matthias, V., Bieser, J., Aulinger, A., and Quante, M.: Sensitivity of modeled atmospheric nitrogen species and nitrogen deposition to variations in sea salt emissions in the North Sea and Baltic Sea regions, Atmos. Chem. Phys., 16, 2921–2942, doi:10.5194/acp-16-2921-2016, http://www.atmos-chem-phys.net/16/2921/2016/, 2016.

Ovadnevaite, J.: personal communication, 2015.

Ovadnevaite, J., Manders, A., de Leeuw, G., Ceburnis, D., Monahan, C., Partanen, A.-I., Korhonen, H., and O'Dowd, C. D.: A sea spray aerosol flux parameterization encapsulating wave state, Atmos. Chem. Phys., 14, 1837–1852, doi:10.5194/acp-14-1837-2014, http://www.atmos-chem-phys.net/14/1837/2014/, 2014.

Sharqawy, M. H., Lienhard, J. H., and Zubair, S. M.: Thermophysical properties of seawater: a review of existing correlations and data, Desalin. Water Treat., 16, 354–380, doi:10.5004/dwt.2010.1079, http://web.mit.edu/lienhard/www/Thermophysical_properties_of_seawater-DWT-16-354-2010.pdf, 2010.

Smith, M. H., Park, P. M., and Consterdine, I. E.: Marine aerosol concentrations and estimated fluxes over the sea, Q. J. Roy. Meteor. Soc., 119, 809–824, doi:10.1002/qj.49711951211, http://dx.doi.org/10.1002/qj.49711951211, 1993.

Spada, M., Jorba, O., Pérez García-Pando, C., Janjić, Z., and Baldasano, J. M.: Modeling and evaluation of the global sea-salt aerosol distribution: sensitivity to size-resolved and sea-surface temperature dependent emission schemes, Atmos. Chem. Phys., 13, 11 735–11 755, doi:10.5194/acp-13-11735-2013, http://www.atmos-chem-phys.net/13/11735/2013/, 2013.

Wu, J.: Wind-stress coefficients over sea surface from breeze to hurricane, J. Geophys. Res. Oceans, 87, 9704–9706, doi:10.1029/JC087iC12p09704, http://dx.doi.org/10.1029/JC087iC12p09704, 1982.